Volume 4
Number 12
December 2024
Pages 1325–1436

Environmental Science
Atmospheres

rsc.li/esatmospheres

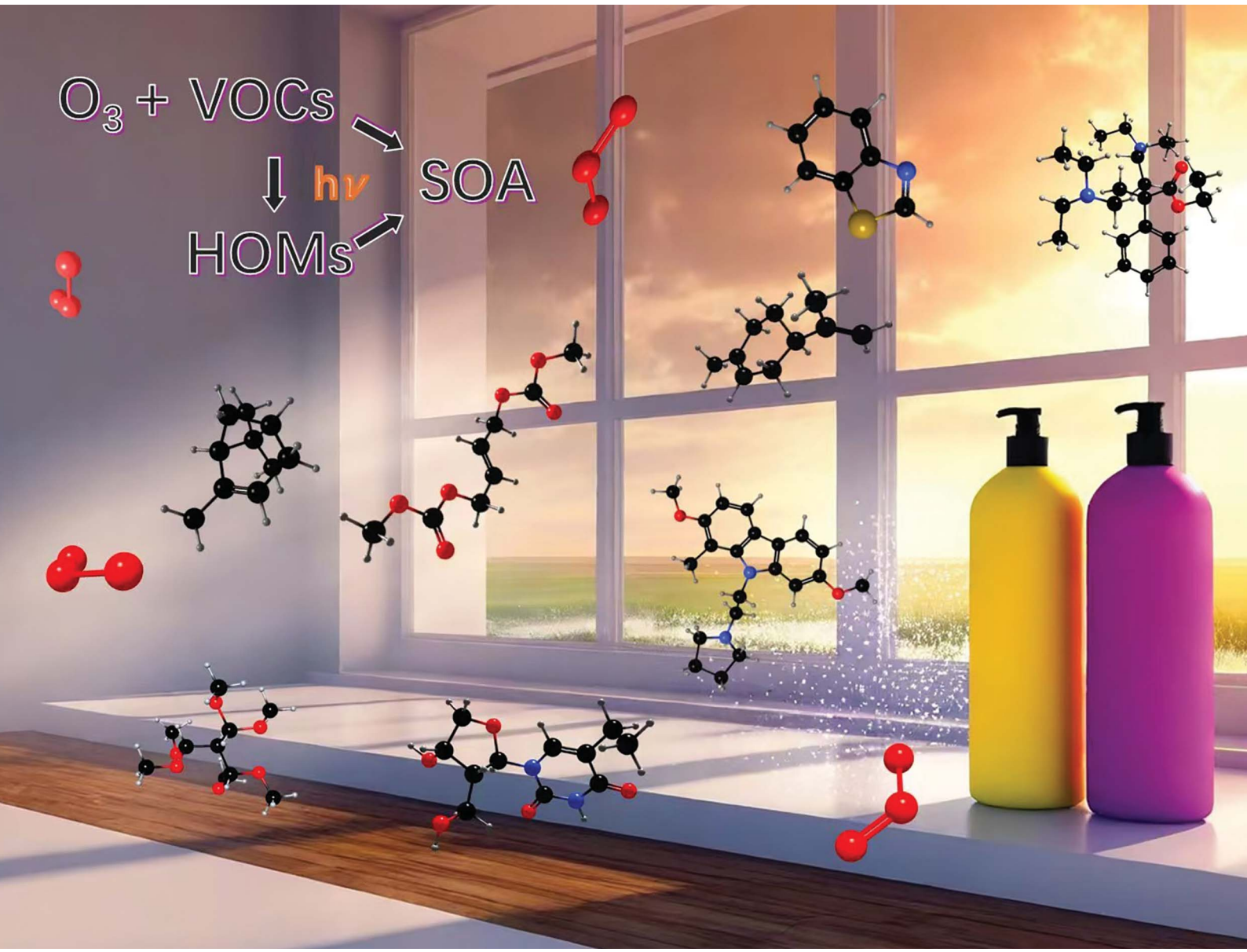

ISSN 2634-3606

ROYAL SOCIETY OF CHEMISTRY

PAPER
Weiwei Hu, Sasho Gligorovski *et al.*
Nitrogen-containing organic aerosols and highly oxidized molecules produced by reaction of ozone with floor cleaning detergent

Environmental Science: Atmospheres

ROYAL SOCIETY OF CHEMISTRY

PAPER

View Article Online
View Journal | View Issue

Cite this: *Environ. Sci.: Atmos.*, 2024, **4**, 1358

Nitrogen-containing organic aerosols and highly oxidized molecules produced by reaction of ozone with floor cleaning detergent†

Jinli Xu,‡[abcd] Tianle Pan,‡[abcd] Tingting Feng,[abcd] Yingkun Wang,[abcd] Wei Chen,[abcd] Weiwei Hu*[abc] and Sasho Gligorovski*[abce]

Cleaning detergents are a source of numerous volatile organic compounds (VOCs) which are highly reactive towards ozone leading to the formation of secondary organic aerosols (SOA) in indoor environments. Here we perform real-time measurements of the organic composition of aerosols produced upon ozone reaction with floor cleaning detergent by extractive electrospray ionization time-of-flight mass spectrometer (EESI-TOF-MS) coupled to a chamber reactor. The experiments were performed in the absence of light and under light irradiation (320 nm < λ < 400 nm) simulating the fraction of sunlight that penetrates indoors. The multiple increases in particle number concentrations correspond to rise in the signal intensity of specific species. Notably, the secondary increase in particle mass concentration is mainly contributed by highly oxidized molecules (HOMs), which increased from 16.5% upon ozone oxidation to 19.9% under photo-oxidation reactions. A large fraction of CHON compounds such as imidazole, pyrazine/pyrimidine, and azaindole was observed most likely formed through the reaction of O_3 with benzothiazole (constituent of the cleaning detergent). The difference between the molecular compositions detected in the absence of light and in the presence of light indicates that sunlight penetrating through the windows can affect the SOA produced by the reaction of ozone with the floor cleaning detergent.

Received 4th June 2024
Accepted 31st October 2024

DOI: 10.1039/d4ea00076e

rsc.li/esatmospheres

Environmental significance

Secondary organic aerosols in the indoor air play an important role from a health point of view but the knowledge about their formation processes and chemical composition is still lacking. Cleaning agents which are widely used indoors represent a source of volatile organic compounds especially monoterpenes which are highly reactive toward ozone and produce organic aerosols. Understanding the formation and chemical structure of these aerosols in particular under sunlight irradiation which penetrates indoors through glass windows is essential for proper modeling of indoor air quality and a comprehensive understanding of their effect on human health.

1 Introduction

Ozone (O_3) reactions in indoor environments have attracted great attention among the scientific community.[1–4] Previous studies have shown that ozone can be generated indoors by photocopiers, laser printers, ozone-based air purifiers, and ozone disinfection cabinets or transported from outdoors through ventilation.[5–7] The indoor O_3 concentration can vary from a few ppb to tens of ppb.[2,8–10] The reactions of O_3 with unsaturated compounds *e.g.* terpenes lead to the formation of secondary organic aerosols (SOA).[1,11–13] In the indoor environment, floor cleaning detergents contain various volatile organic compounds (VOCs) including terpenes and terpenoids which can react rapidly with ozone to generate aerosol particles.[1,14–19] Few studies have shown that use of cleaning products, indeed leads to the formation of SOA in the indoor air.[1,17,18,20] One of the main constituents of the cleaning products is D-limonene which concentration in the indoor air can reach up to 13 ppb during the cleaning event.[17] Another study showed that α-pinene, D-limonene, and β-pinene, which are important ingredients in detergents,[19] can lead to a significant increase (~15%) in particulate matter within three hours after the cleaning event

[a]*State Key Laboratory of Organic Geochemistry, Guangdong Provincial Key Laboratory of Environmental Protection and Resources Utilization, Guangzhou Institute of Geochemistry, Chinese Academy of Sciences, Guangzhou 510640, China. E-mail: weiweihu@gig.ac.cn; gligorovski@gig.ac.cn*

[b]*Guangdong-Hong Kong-Macao Joint Laboratory for Environmental Pollution and Control, Guangzhou Institute of Geochemistry, Chinese Academy of Science, Guangzhou 510640, China*

[c]*Chinese Academy of Science, Centre for Excellence in Deep Earth Science, Guangzhou 510640, China*

[d]*University of Chinese Academy of Sciences, Beijing 101408, China*

[e]*University St. Kliment Ohridski Bitola, Boulevard 1st of May B.B., Bitola 7000, North Macedonia*

† Electronic supplementary information (ESI) available. See DOI: https://doi.org/10.1039/d4ea00076e

‡ The first two authors contribute equally.

compared to no cleaning activities.[21] The gas-phase emission from the cleaning detergent used in our study contains more than 30 volatile organic compounds (VOCs), including D-limonene and a variety of alcohols (dihydromyrcenol, γ-terpineol, α-terpineol) and esters (2-hydroxypropyl methacrylate and allyl heptanoate).[19] These compounds have the potential to react with ozone and produce secondary organic aerosols (SOA).[22,23] It has been found that the reaction of ozone with D-limonene produces more SOA particles than its reaction with α-pinene,[24–26] however, it is α-pinene that exhibits higher aerosol formation potential in terms of ozone reactivity.[27,28]

Over the past two decades, extensive research has been conducted on the chemical composition of secondary organic aerosols (SOA) produced through the ozonolysis of terpenes, with a particular emphasis on the mass and number concentrations as well as the size distribution of the particles generated during indoor cleaning activities.[1,20,29–38] Furthermore, several studies have delved into the SOA formation resulting from specific reactants, such as limonene, α-pinene, ozone, and nitrogen oxides (NOx).[31–33,35] These investigations have also incorporated methodologies that involve the collection of filter samples and the application of various offline analytical techniques to identify the chemical constituents of the particulate phase.[29] Despite this extensive body of work, our understanding of the composition of indoor-generated SOA remains incomplete. This knowledge gap is significant, especially considering the implications for human health.[20,38–42] Indeed, it has been shown that the deposited aerosol dose in the particle range of 1.2–800 nm, formed by the ozonolysis of monoterpenes during the mopping event is greater than, or comparable to, that one would inhale in an urban street canyon traffic.[1,43,44]

In the present investigation, we conducted a real-time assessment of aerosol particle formation following the reaction between gaseous ozone (O_3) and a commonly utilized floor-cleaning detergent. This study was designed to simulate indoor environmental conditions, examining scenarios both devoid of light and exposed to UV-light within the range typical for indoor settings (320 nm < λ < 400 nm).[10,45–47] The aerosols generated through the ozonolysis of the cleaning detergent were characterized using an extractive electrospray ionization time-of-flight mass spectrometer (EESI-TOF-MS), which provided insights into their chemical composition. Concurrently, particle size distributions were determined utilizing a scanning mobility particle sizer (SMPS), with measurements recorded every 4 minutes. Experimental observations indicated that particulate matter mass concentrations varied from 5 to 7 μg m^{-3}, with an increase attributed to secondary particle formation during photo-oxidation reactions (Fig. S1†).

2 Materials and methods

2.1 Set up of the reactor

The experiments were carried out in a spherical borosilicate glass reactor ($R = 9$ cm, $V = 3.05$ L) (Fig. S3†). The glass reactor was placed in a stainless-steel box equipped with eight UV-A lamps (40 W, 320 nm < λ < 400 nm) simulating the sunlight intensity penetrating indoors.[10,45,46] A flow of 100 mL min^{-1} (range 0–200 mL min^{-1} HORIBA METRON mass flow controller; accuracy, ±1%) tank zero air passed through a commercial ozone generator (UVP, LLC Upland) to produce a stable mixing ratio of O_3. Another flow of 500 mL min^{-1} air (0–500 mL min^{-1} HORIBA METRON mass flow controller; accuracy, ±1%) passed through a glass bottle filled with bubbling ultrapure water (18 M-ohm, H2OMM-UV-T, Germany) to control the relative humidity (RH). These two flows were mixed to acquire the O_3 mixing ratios of 50 ± 5 ppb, simulating the ozone levels in an indoor environment with the 70% RH and then introduced into the reactor through the right exit. The left exit of the reactor is connected to a diluted airflow of 1.7 L min^{-1} (0–5 L min^{-1} HORIBA METRON mass flow controller; accuracy, ±1%) before introducing it into a scanning mobility particle sizer (SMPS) and an extractive electrospray ionization time-of-flight mass spectrometer (EESI-TOF-MS, ToFWerk AG and Aerodyne Research Inc.) (Fig. S3†). The preparation of the samples is described in the ESI.† Particle composition was measured by EESI-TOF-MS. Particle mass concentration and size distributions were measured by a scanning mobility particle sizer (SMPS, 3080, TSI Inc.). Our study specifically examines the impact of varying ozone reaction conditions on the composition of particles in the aerosol phase.

2.2 Extractive electrospray ionization time-of-flight mass spectrometer (EESI-TOF-MS)

The EESI-TOF-MS is a commercial instrument (ToFWerk AG and Aerodyne Research Inc.) coupled with positive electrospray ionization (ESI^+) sources.[48] The aerosols were sampled using an activated carbon denuder (2 cm diameter, 4 cm height, with a 1 mm square aperture) at a flow rate of 0.37 L min^{-1}, before encountering a droplet spray from a fused silica electrospray capillary (360 μm outer diameter and 75 μm inner diameter). The extraction solvent, a 50 : 50 mixture of water and acetonitrile, was fortified with 100 ppm of sodium iodide (NaI) to facilitate the detection of aerosol molecules. The soluble constituents of the aerosol were effectively captured within the liquid phase. As the droplets evaporated, the resulting compounds were characterized as sodium ion (Na^+) adducts. The adducts were guided through a series of ion guides and were separated based on their mass-to-charge ratio in a time-of-flight mass spectrometer. During the experiments, the resolution of the mass spectrometer was $m/\Delta m \sim 9000$–10 000. Positive ion spectra were recorded at a time resolution of 5 s and were averaged to a 1 min resolution in the latter analysis. Continuous background measurements were conducted by periodically sampling aerosols through a particulate filter (Balston disposable filter unit, model Parker 9933-11-BQ, USA) for 3 minutes within every 12 minute interval.[33] After switching from the sampling line to the filter or filter to the sampling line, transition data (~1 min) were recorded, which was deleted to exclude the interferences. $[(NaI)_n]Na^+$ clusters are also removed from the dataset. Before the experiments, we calibrated the EESI-TOF-MS for levoglucosan, achieving a detection limit of 16.4 ng m^{-3} and a sensitivity of 2283.1 ions per s μg m^3. No matrix effect was found in our study, which is consistent with

what Lopez-Hilfiker *et al.* (2019) found.[48] The description of the data analysis by EESI-TOF-MS is shown in the ESI.†

3 Results and discussion

3.1 Hierarchical cluster analysis

Fig. 1 shows the hierarchical cluster analysis performed by Matlab R2018b to identify the compounds with different chronological variations during ozone-only, simultaneous ozone and light, and light-only, exposure periods.

The hierarchical cluster diagram (HKD) obtained from real-time monitoring of 194 selected ions was classified into four groups that exhibit different signal intensity–time profiles. The grouping lines of the clusters were shown in the left of Fig. 1A. The groups marked with a blue and green rectangle contain 26 and 25 species, respectively, and show increasing intensity trends (Fig. 1A and B) as the floor-cleaning detergent was exposed to O_3. The intensity of the species categorized under 'Blue' diminishes when the detergent is concomitantly subjected to ozone (O_3) and light exposure, signifying that these species are likely consumed during the photo-oxidation process. Conversely, the ion intensity within the 'Green' group increases upon both ozone-only and photo-oxidation reactions. Additionally, the 'Blue' and 'Green' groups can be further differentiated into multiple sub-groups, as illustrated in ESI, Fig. S4 and S5.† The 'Yellow' group predominantly display an increase in ion intensity under photo-oxidation conditions with the cleaning detergent while the ion signals in the 'Red' group increase under both reaction conditions (Fig. S6†). However, the evolutionary trend of species in the 'Red' group is significantly distinct from that in the 'Green' group. Fig. 1C presents a comparative analysis of the ion intensities across all four groups under the two experimental scenarios. The 'Yellow' and 'Red' groups are predominantly composed of dimers with carbon chains ranging from C15 to C20 or even larger. In contrast, the 'Blue' and 'Green' groups are comprised of monomers with shorter carbon chains, C5 to C10. The majority of compounds within the 'Blue' group exhibit a O/C $\leq$ 0.5, and H/C $\geq$ 1.5, suggesting that aliphatic hydrocarbons are the predominant constituents. Both 'Yellow' and 'Red' groups may also include aliphatic hydrocarbons, as indicated by their H/C and O/C ratios that fall within the ranges of 1.70 to 2.13 and 0 to 0.42, respectively. Contrasting these, the 'Green' group is primarily composed of highly oxidized functional compounds (28%) along with a significant proportion of aliphatic hydrocarbons (16.0%).[49–51] In the following section, is provided a detailed introduction to classifications of the observed substances.

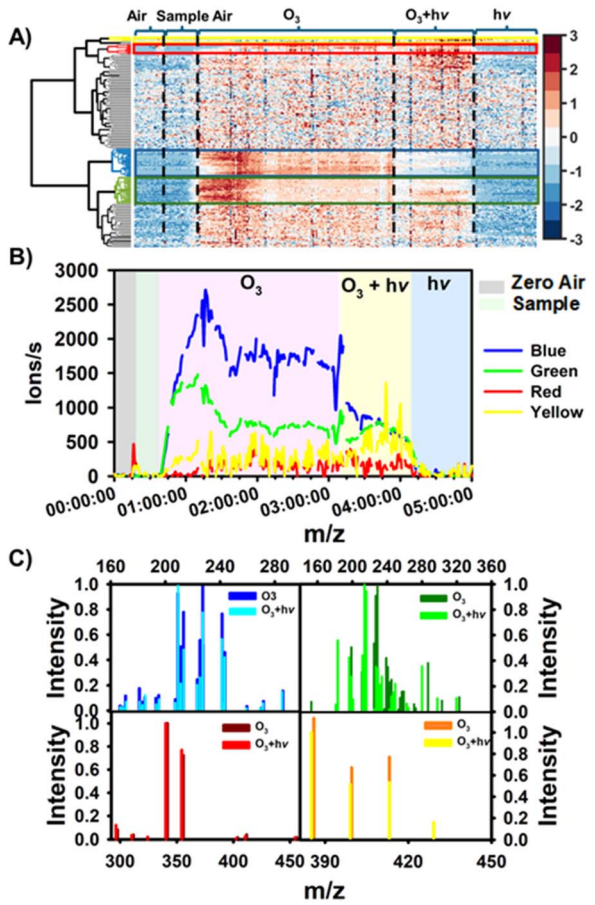

Fig. 1 (A) Hierarchical cluster analysis of 194 ions detected by EESI-TOF-MS upon ozone oxidation reaction and photo-oxidation reaction. The grouping lines of the clusters are shown in the left. The normalized signal intensity in the hierarchical cluster is presented by a color-coded scale; *i.e.,* the signal intensity increases linearly from dark blue (normalized value of −3) to wine red (normalized value of 3). (B) Curves showing signal intensity over time for different groups derived from hierarchical cluster analysis. (C) Mass spectra of observed ions in four groups produced under oxidation reaction (dark color) and photo-oxidation reaction (light color). The signal is normalized to the maximum of the highest peak in the group.

3.2 Mass spectral analysis

Fig. 2 shows the high-resolution mass spectra (background-subtracted) of the observed species produced under different conditions. For sake of convenience all substances in the text are shown solely in the form of organic molecular formulas excluding the Na^+ ion. The mass spectra depicted in Fig. 2 represent the average profiles for each distinct phase of the reaction: namely, ozone oxidation (Fig. 2A), photo-oxidation reactions (Fig. 2B), and the differences between them (Fig. 2C). In the first two mass spectra (Fig. 2A and B), the ion signal intensities are normalized to the highest peak observed under the respective reaction conditions. Fig. 2C is derived by subtracting the ion signals depicted in Fig. 2B (photo-oxidation) from those in Fig. 2A (ozonolysis), thereby highlighting the differences in the products formed under different reaction conditions. Among all the detected compounds, both monomers (C5–C10) and dimers (C15–C20) are evident (Fig. 2A and B).[19] The monomer region is dominated by C9 and C10 species, which together account for 71.4% of the total detected monomer compounds formed upon ozone oxidation reactions, and 66.1% produced during photo-oxidation reactions. In our previous study[19] focused on the heterogenous chemistry of ozone on floor-cleaning detergent, the majority of the detected compounds were monomers retaining the skeleton of VOCs

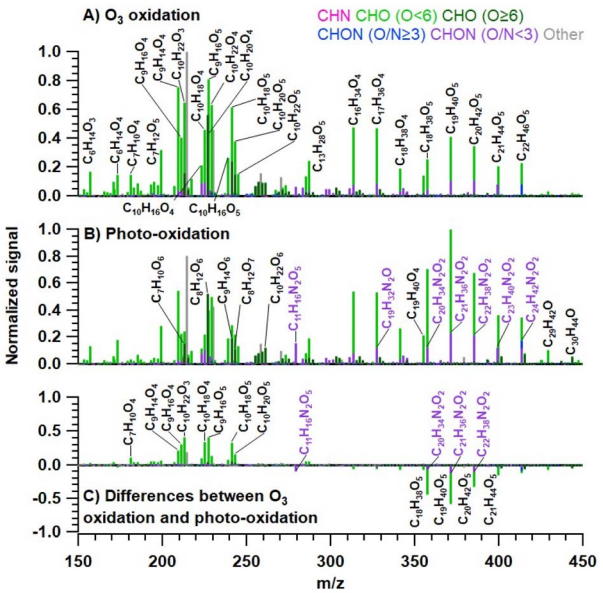

Fig. 2 High-resolution mass spectra of the observed species produced under (A) ozone oxidation reaction, (B) photo-oxidation oxidation reaction, and (C) comparison of both spectra calculated by graph (A) minus graph (B). The signal is normalized to the maxima of the highest peaks observed. Due to space constraints, only the species with the highest relative signal intensity are labelled in this figure. The labelled species in the figure have omitted the Na^+ ion.

(C7–C10), but here products with different C-numbers were also observed. The photo-oxidation reaction is notably characterized by an increase in the average molecular size, attributable to the condensation process and the incorporation of monomers into oligomeric structures. In particular, dimers (C15–C20) and higher-molecular weight oxygenated compounds are formed as shown on the negative axis, while monomers (C5–C10) have been consumed as shown on the positive axis (Fig. 2C). Note that the CHON (O/N < 3) compounds in the generated dimers have increased significantly, which will be discussed in detail in the later 'CHON compounds' section.

In order to further distinguish the differences in oxidation products under various reaction conditions, here we subdivided the CHO and CHON compounds (for more details see section "CHON compounds") into five groups according to their carbon oxidation states (OSc) and corresponding H/C and O/C ratios, as follows: aliphatic compounds which can be cyclic, saturated, and unsaturated compounds, ($H/C \geq 1.5$, $O/C \leq 0.5$);[52,53] low oxidized aromatic compounds *e.g.* unsaturated low-oxygen-containing aromatic hydrocarbons, ($H/C \leq 1.0$, $O/C \leq 0.5$);[54] highly oxidized functional compounds *e.g.* alcohols, esters, and peroxides, ($OSc \geq 0$, $O/C \geq 0.6$); highly reduced functional compounds like organic acids and carbonyls, ($OSc < 0$, $O/C \geq 0.6$); and moderately oxygenated compounds, ($OSc \geq 0$, $O/C \geq 0$ and $H/C \leq 1.2$).[49–51] It should be noted that the majority of CHO compounds under all conditions are aliphatic in nature, constituting over 50% of the observed species. These are followed in prevalence by highly oxidized functional compounds, which account for approximately 15%, and highly reduced functional compounds, which make up about 10%. Relative to the ozone reactions conducted in the dark, the photo-oxidation reactions exhibit a reduced production of aliphatic compounds and an increased presence of both highly oxidized and highly reduced functional compounds, as illustrated in Fig. S12.†

Another very interesting finding is that the formation of HOMs appears to be correlated with the evolution trend of particulate matter. HOMs are distinguished by elevated O/C ratios, falling within the range of 0.4 to 1.1, and contain a minimum of six oxygen atoms in their molecular structures.[55] They constitute 16.5% and 19.9% of the total compounds generated during the ozone oxidation and photo-oxidation processes, respectively. These species are hypothesized to originate from auto-oxidation reactions.[55] Consequently, they are considered to represent an upper estimate of the HOMs yield.[56–60] In this study, we report a significant increase in the normalized signal intensity of numerous HOMs observed during both oxidation and photo-oxidation reactions. The observed increase in HOMs concentration under light conditions aligns with the established research conclusion that ultraviolet light further stimulates auto-oxidation reactions.[61–66] The highly oxidized organic compounds produced from ozone oxidation can nucleate, accumulate, and grow SOA.[35,67,68] Taking the 'Green' group as an example, 56% of the species can be classified as HOMs, and the signal intensity of these species has increased again under photo-oxidation conditions (Fig. S5†). However, except for $C_{10}H_{20}O_6$, the signal intensity of other ions rapidly declines after reaching their peak, while the particle mass concentration subsequently reaches a second peak, which coincides with the increase in signal intensity of higher molecular weight species in the 'Yellow' group (Fig. S7†). We posit that the consumption of these HOMs and the formation of larger species, to a significant degree, are responsible for the secondary increase in mass concentration (Fig. S1†). Furthermore, our analysis of data shown in Fig. S2† suggests that the secondary increase in particulate matter mass concentration under photo-oxidation conditions is primarily attributed to the enlargement of existing particles with a diameter of 60–300 nm formed by oxidation reactions, rather than the formation of new particles. Furthermore, the multiple increases in particle number concentration are in harmony with the evolution trend of aerosol species. To elaborate, the first increase in particle concentration (red section) in Fig. S2A† corresponds to the explosive increase in signal intensity of the 'Blue' and 'Green' groups in Fig. S2B.† The second and third increases in particle concentration during the oxidation reaction phase in Fig. S2A† correspond to the two slight increases in signal intensity of the 'Blue' and 'Green' groups in Fig. S2B.† The last increase in particle concentration during the photo-oxidation reaction phase in Fig. S2A† corresponds to the significant increase in signal intensity of the 'Yellow' group in Fig. S2B.† This corresponding phenomenon to some extent indicates that the increase in the intensity of the ion signals shown in Fig S2B† is contributed by the particulate matter that formed first in Fig S2A.†

The aforementioned differences in the molecular composition of aerosols highlight the potential impact of sunlight penetrating through windows in indoor settings. Specifically, it

suggests that the secondary organic aerosols (SOA) generated from the interaction between ozone and the surface treated with floor cleaning detergent are subject to modification by natural sunlight.

A van Krevelen (VK) diagram of the detected CHO compounds is illustrated in Fig. S8† in the form of H/C *versus* O/C, showing different types of compounds within the same CH_2 homologous series. The relative number abundances of the compounds produced under different conditions are shown in the pie chart in Fig. S9.† There are 43 groups of CHO compounds with different numbers of CH_2 groups shown in Fig. S8,† exhibiting a broad range of DBE values from 0 to 11. The specifics regarding the data presented in Fig. S9,† as well as the categorization of these compounds, are delineated in Table S2.† Compounds are categorized based on parameters such as O/C, H/C, DBE, and X_C. Please refer to ESI† for more information about DBE and X_C. In short, DBE refers to double bond equivalent, representing the degree of unsaturation of compounds while X_C, the aromaticity equivalent, serves as a supplement to DBE. In particular, CHO compounds with a DBE of 0 are identified as saturated alcohols or ethers; compounds with $X_C = 0$ are unsaturated aliphatic compounds; compounds with $0 < X_C < 2.5$ are unsaturated aliphatic compounds or cyclic compounds, and compounds with $X_C \geq 2.5$ are suggestive of aromatic or polycyclic structures, potentially featuring multiple unsaturated functional groups or rings.

As shown in Fig. S10,† most of the identified compounds are in the SVOC (45.1%, $-0.5 < \log\ C \times \leq 2.5$) and IVOC (36.4%, $2.5 < \log\ C \times \leq 6.5$) ranges, and almost no compounds in the ELVOC range (3.28%) (see text S6† for details of the classification).

3.3 CHON compounds

We also detected CHON product compounds during the reaction of O_3 with the floor-cleaning detergent whose precursor is most likely benzothiazole (C_7H_5NS),[19] among the others. It has been shown that the reaction of O_3 with azoles leads to the formation of nitrosamines which are then transformed to higher molecular weight N-heterocyclic compounds.[69–71] Since EESI-TOF-MS of the Na^+ ion source is mainly sensitive to CHON compounds and cannot detect compounds containing S,[48,72] no products containing S were observed. There are 40 groups of CHON compounds with different CH_2 group numbers shown in Fig. 3 and exhibit a broad range of DBE values from 0 to 14. The CHON compounds with $0 < X_C < 2.5$ should contain at least a nitro- ($-NO_2$), amine group, or nitroso – ($-N{=}O$) group.[73] CHON compounds with $2.5 \leq X_C < 2.7143$ are likely aromatics with a benzene core structure containing nitrogen functional groups, or nitrogen-containing heterocyclic compounds.[74] Compounds with $X_C \geq 2.7143$ are condensed aromatic hydrocarbon.[75] To facilitate an extensive yet concise presentation of data, Table S2 in the ESI† offers an elaborate breakdown of the compounds depicted in Fig. 3 The table includes specific DBE and X_C values, alongside potential functional groups attributed to each compound class.

The comparative analysis of compound production, as depicted in Fig. S9,† indicates that the ozone reaction with the detergent yields a higher abundance of saturated compounds with DBE = 0 than those generated through the photo-oxidation process. Conversely, other compounds are more prevalent in the photo-oxidation scenario.

The photo-oxidation reaction is characterized by a richer diversity of functional compounds. These include highly reduced species (OSc < 0, O/C ≥ 0.6) and highly oxidized functional compounds (OSc ≥0, O/C ≥ 0.6). The presence of low-oxidized aromatic compounds is also notable, identified by hydrogen-to-carbon (H/C) ratios not exceeding 1.0 and an O/C ratio not surpassing 0.5.

Furthermore, the photo-oxidation reaction, in contrast to the reaction conducted in the dark, is marked by a higher yield of moderately oxidized compounds, characterized by an O/N ratio within the range of 0 to 3. This observation is complemented by a notable increase in relative signal intensity of reduced CHON compounds (O/N < 3) under photo-oxidation reaction as shown in Fig. 2, and the decrease in CHN substances depicted in Fig. S11.†

Within the CHN compound group, the most prevalent subset comprises molecules with two nitrogen atoms (N_2) and DBE value exceeding 5. Notably, the series of homologous compounds, such as $C_{12}H_{16}N_2(CH_2)_n$, $C_{12}H_{14}N_2(CH_2)_n$, $C_{14}H_{10}N_2(CH_2)_n$, and $C_{14}H_8N_2(CH_2)_n$, are tentatively identified as belonging to the imidazole, pyrazine/pyrimidine, and azaindole chemical classes.[76,77] The formation of CHON compounds with O/N = 0.5, produced by ozone reaction and photo-oxidation reaction with the floor detergent, suggests the presence of nitrosamines which could be also formed as second-generation products by ozone oxidation of N-heterocycle compounds such as imidazoles.[69,78] Similarly, the high intensity of compounds with O/N = 1 produced during the photo-oxidation reaction, could result from light-induced ozone reaction of first-generation products (N-heterocyclic aromatic compounds), such as imidazole, pyrazole,[69,78] piperidine, piperazine and quinoline, or compounds containing amide group. For compounds with more abundant O-atoms, it has been reported that CHON compounds with O/N < 3 are more likely to incorporate nitrogen-containing and oxygen-containing groups.[79] Conversely, CHON compounds with an O/N ratio ≥ 3 are postulated to contain groups consisting of both nitrogen and oxygen, such as nitrite ($-NO_2$), nitrate ($-NO_3$), and nitrooxy ($-ONO_2$) functional groups. The presence of these groups in the studied compounds implies the formation of nitrooxy ($-ONO_2$) amines, imines, or organonitrates in this study.[80–83] This inference is supported by our previous findings on riverine surface microlayer, where these compounds were identified as tertiary products resulting from the ozonolysis of secondary N-heterocycle compounds, such as imidazole.[70,71] However, the underlying reaction mechanism remains elusive at this stage, and elucidating the molecular-level formation of these compounds presents a formidable challenge. This difficulty is particularly pronounced when authentic samples are utilized instead of proxy compounds. Nevertheless, we propose that the N-containing compounds present in the detergent act

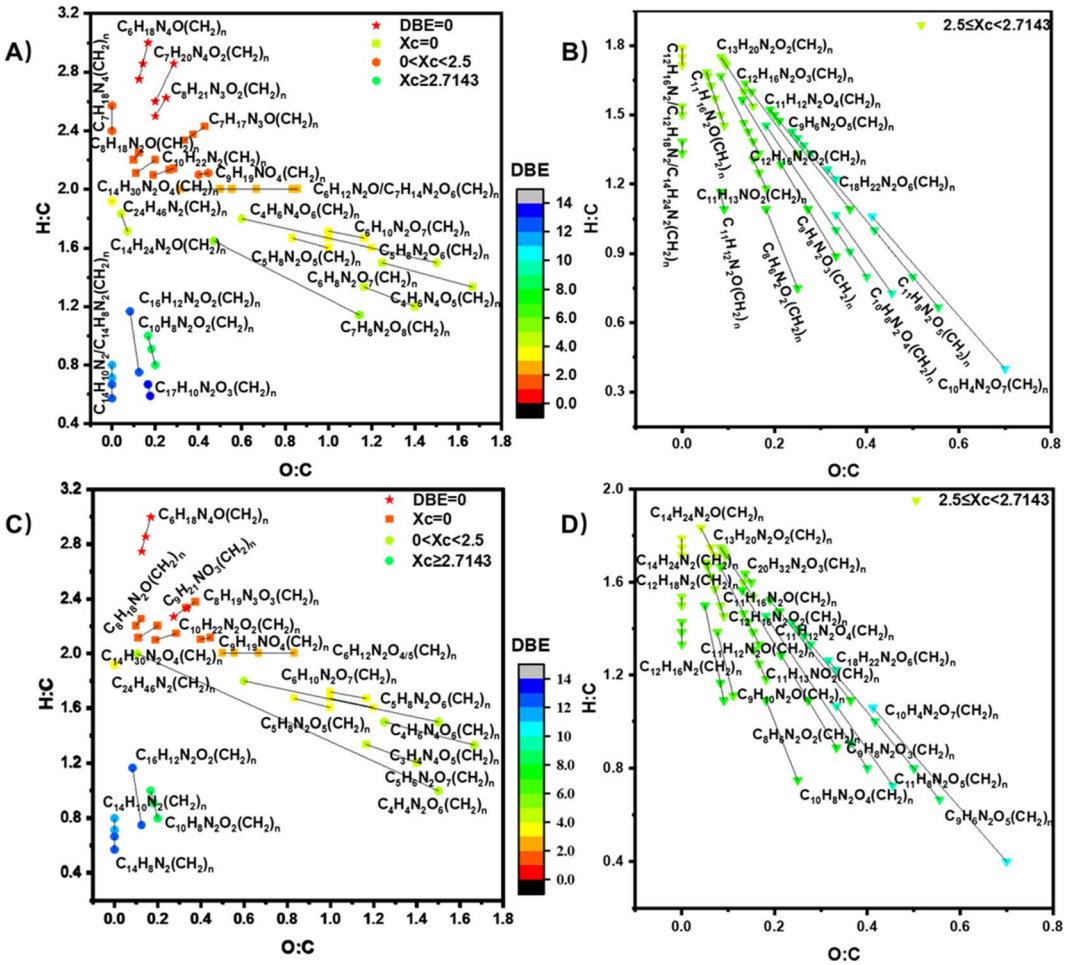

Fig. 3 Van Krevelen plot for homologous series of CHON compounds produced from the ozone oxidation reaction (A and B) and photo-oxidation reaction (C and D). The "*n*" refers to the number of CH_2 groups in a given family.

as precursors to the CHON product compounds, given that no NOx species were involved in the reaction process.

4. Conclusions

Considering that in a real-life indoor environment, there is the presence of other oxidants/reactants such as NO_2, NO_3, and NH_3, the number and mass concentration of the particles generated from the use of cleaning detergent may be significantly higher than those observed in this study under laboratory conditions.[16,84–87] The highly oxidized organic compounds produced from ozone oxidation can nucleate, accumulate, and grow SOA.[11,35,67] It has been reported that people would inhale approximately 3.8×10^{10} to 1.8×10^{11} particles (3.0 to 7.5 μg) over the duration of a 90 min indoor mopping event, with much of the inhalation intake occurring during the first few minutes of active cleaning.[1] Therefore, it is necessary to further understand the evolution trend of particle size and composition of particulate matter produced by the reaction between ozone and common floor detergents.

In particular, the formation of nitrogen-containing aerosols may exacerbate indoor air quality and affect human health. Here, we observed the formation of imidazole, pyrazine/pyrimidine, and azaindole compounds, which are likely to be formed by the oxidation of ozone with benzothiazole, a constituent of the floor detergent. It has been shown that imidazoles are potentially toxic compounds.[88] Therefore, from a health point of view, it is strongly recommended future studies evaluate the combined effect of oxidants on the particle formation by ozone chemistry of cleaning products in indoor environments.

Data availability

The data supporting this article have been included as part of the ESI.†

Author contributions

WH and SG conceived the study and designed the overall scope. JX, and TP performed the experiments and analysed the data. JX, TP, WH, and SG wrote the manuscript. TF, YW, and WC, participated in the experiments and engaged in scientific discussions regarding the manuscript.

Conflicts of interest

There are no conflicts to declare.

Acknowledgements

This study was financially supported by National Natural Science Foundation of China, Research Fund for International Scientists (4221101064), National Natural Science Foundation of China (42177087, 42230701, 42375105), Science Fund for Creative Research Groups of the National Natural Science Foundation of China (42321003), Ministry of Science and Technology of China (2022YFC3701102), and the Guangdong Foundation for Program of Science and Technology Research (2023B1212060049). Weiwei Hu was supported by the Guangdong Pearl River Talents Program (2019QN01L948).

Notes and references

1 C. M. F. Rosales, J. L. Jiang, A. Lahib, B. P. Bottorff, E. K. Reidy, V. Kumar, A. Tasoglou, H. Huber, S. Dusanter, A. Tomas, B. E. Boor and P. S. Stevens, Chemistry and human exposure implications of secondary organic aerosol production from indoor terpene ozonolysis, *Sci. Adv.*, 2022, **8**, eabj9156.

2 W. W. Nazaroff and C. J. Weschler, Indoor ozone: concentrations and influencing factors, *Indoor Air*, 2022, **32**, e12942.

3 C. J. Weschler and W. W. Nazaroff, Ozone Loss: A Surrogate for the Indoor Concentration of Ozone-Derived Products, *Environ. Sci. Technol.*, 2023, **57**, 13569–13578.

4 Y. J. Liu, P. K. Misztal, C. Arata, C. J. Weschler, W. W. Nazaroff and A. H. Goldstein, Observing ozone chemistry in an occupied residence, *Proc. Natl. Acad. Sci. U.S.A.*, 2021, **118**(6), e2018140118.

5 Q. Zhang and P. L. Jenkins, Evaluation of ozone emissions and exposures from consumer products and home appliances, *Indoor Air*, 2017, **27**, 386–397.

6 H. Salonen, T. Salthammer and L. Morawska, Human exposure to ozone in school and office indoor environments, *Environ. Int.*, 2018, **119**, 503–514.

7 C. J. Weschler, Ozone in indoor environments: Concentration and chemistry, *Indoor Air*, 2000, **10**, 269–288.

8 A. Wisthaler and C. J. Weschler, Reactions of ozone with human skin lipids: sources of carbonyls, dicarbonyls, and hydroxycarbonyls in indoor air, *Proc. Natl. Acad. Sci. U.S.A.*, 2010, **107**, 6568–6575.

9 S. Zhou, C. J. Young, T. C. VandenBoer and T. F. Kahan, Role of location, season, occupant activity, and chemistry in indoor ozone and nitrogen oxide mixing ratios, *Environ. Sci.: Processes Impacts*, 2019, **21**, 1374–1383.

10 J. Liu, S. Li, J. Zeng, M. Mekic, Z. Yu, W. Zhou, G. Loisel, A. Gandolfo, W. Song, X. Wang, Z. Zhou, H. Herrmann, X. Li and S. Gligorovski, Assessing indoor gas phase oxidation capacity through real-time measurements of HONO and NOx in Guangzhou, China, *Environ. Sci.: Processes Impacts*, 2019, **21**, 1393–1402.

11 N. Carslaw, A mechanistic study of limonene oxidation products and pathways following cleaning activities, *Atmos. Environ.*, 2013, **80**, 507–513.

12 C. J. Weschler and H. C. Shields, Indoor ozone/terpene reactions as a source of indoor particles, *Atmos. Environ.*, 1999, **33**, 2301–2312.

13 K. Pytel and B. Zabiegala, Investigation of RH effect on uncommon limonene ozonolysis products and SOA formation in indoor air with real time measurement techniques, *Chemosphere*, 2024, **349**, 140854.

14 H. Destaillats, M. M. Lunden, B. C. Singer, B. K. Coleman, A. T. Hodgson, C. J. Weschler and W. W. Nazaroff, Indoor Secondary Pollutants from Household Product Emissions in the Presence of Ozone: A Bench-Scale Chamber Study, *Environ. Sci. Technol.*, 2006, **40**, 4421–4428.

15 Y. Huang, K. F. Ho, S. S. H. Ho, S. C. Lee, P. S. Yau and Y. Cheng, Physical parameters effect on ozone-initiated formation of indoor secondary organic aerosols with emissions from cleaning products, *J. Hazard. Mater.*, 2011, **192**, 1787–1794.

16 Y. Huang, S. C. Lee, K. F. Ho, S. S. H. Ho, N. Y. Cao, Y. Cheng and Y. Gao, Effect of ammonia on ozone-initiated formation of indoor secondary products with emissions from cleaning products, *Atmos. Environ.*, 2012, **59**, 224–231.

17 S. Rossignol, C. Rio, A. Ustache, S. Fable, J. Nicolle, A. Meme, B. D'Anna, M. Nicolas, E. Leoz and L. Chiappini, The use of a housecleaning product in an indoor environment leading to oxygenated polar compounds and SOA formation: gas and particulate phase chemical characterization, *Atmos. Environ.*, 2013, **75**, 196–205.

18 A. W. Norgaard, J. D. Kudal, V. Kofoed-Sorensen, I. K. Koponen and P. Wolkoff, Ozone-initiated VOC and particle emissions from a cleaning agent and an air freshener: risk assessment of acute airway effects, *Environ. Int.*, 2014, **68**, 209–218.

19 J. L. Xu, H. F. Deng, Y. Q. Wang, P. Li, J. Q. Zeng, H. W. Pang, X. Xu, X. Li, Y. Yang and S. Gligorovski, Heterogeneous chemistry of ozone with floor cleaning agent: Implications of secondary VOCs in the indoor environment, *Sci. Total Environ.*, 2023, **862**, 160867.

20 L. Stabile, G. De Luca, A. Pacitto, L. Morawska, P. Avino and G. Buonanno, Ultrafine particle emission from floor cleaning products, *Indoor Air*, 2021, **31**, 63–73.

21 N. Carslaw and D. Shaw, Modification of cleaning product formulations could improve indoor air quality, *Indoor Air*, 2022, **32**, e13021.

22 I. Pullinen, S. Schmitt, S. Kang, M. Sarrafzadeh, P. Schlag, S. Andres, E. Kleist, T. F. Mentel, F. Rohrer, M. Springer, R. Tillmann, J. Wildt, C. Wu, D. F. Zhao, A. Wahner and A. Kiendler-Scharr, Impact of NOx on secondary organic aerosol (SOA) formation from α-pinene and β-pinene photooxidation: the role of highly oxygenated organic nitrates, *Atmos. Chem. Phys.*, 2020, **20**, 10125–10147.

23 J. Palmisani, A. W. Norgaard, V. Kofoed-Sorensen, P. A. Clausen, G. de Gennaro and P. Wolkoff, Formation of ozone-initiated VOCs and secondary organic aerosol

following application of a carpet deodorizer, *Atmos. Environ.*, 2020, **222**, 117149.

24 Å. K. Watne, J. Westerlund, Å. M. Hallquist, W. H. Brune and M. Hallquist, Ozone and OH-induced oxidation of monoterpenes: changes in the thermal properties of secondary organic aerosol (SOA), *J. Aerosol Sci.*, 2017, **114**, 31–41.

25 G. Sarwar and R. Corsi, The effects of ozone/limonene reactions on indoor secondary organic aerosols, *Atmos. Environ.*, 2007, **41**, 959–973.

26 M. S. Waring, J. R. Wells and J. A. Siegel, Secondary organic aerosol formation from ozone reactions with single terpenoids and terpenoid mixtures, *Atmos. Environ.*, 2011, **45**, 4235–4242.

27 D. F. Zhao, M. Kaminski, P. Schlag, H. Fuchs, I. H. Acir, B. Bohn, R. Häseler, A. Kiendler-Scharr, F. Rohrer, R. Tillmann, M. J. Wang, R. Wegener, J. Wildt, A. Wahner and T. F. Mentel, Secondary organic aerosol formation from hydroxyl radical oxidation and ozonolysis of monoterpenes, *Atmos. Chem. Phys.*, 2015, **15**, 991–1012.

28 N. Zeinali, I. Oluwoye, M. K. Altarawneh, M. H. Almatarneh and B. Z. Dlugogorski, Probing the Reactivity of Singlet Oxygen with Cyclic Monoterpenes, *ACS Omega*, 2019, **4**, 14040–14048.

29 M. Jaoui, E. Corse, T. E. Kleindienst, J. H. Offenberg, M. Lewandowski and E. O. Edney, Analysis of secondary organic aerosol compounds from the photooxidation of d-limonene in the presence of NOx and their detection in ambient PM2.5, *Environ. Sci. Technol.*, 2006, **40**, 3819–3828.

30 J. K. Nojgaard, A. W. Norgaard and P. Wolkoff, On-line analysis of secondary ozonides from cyclohexene and D-limonene ozonolysis using atmospheric sampling townsend discharge ionization mass spectrometry, *Atmos. Environ.*, 2007, **41**, 8345–8354.

31 S. Leungsakul, M. Jaoui and R. M. Kamens, Kinetic mechanism for predicting secondary organic aerosol formation from the reaction of D-limonene with ozone, *Environ. Sci. Technol.*, 2005, **39**, 9583–9594.

32 M. L. Walser, Y. Desyaterik, J. Laskin, A. Laskin and S. A. Nizkorodov, High-resolution mass spectrometric analysis of secondary organic aerosol produced by ozonation of limonene, *Phys. Chem. Chem. Phys.*, 2008, **10**, 1009–1022.

33 D. M. Bell, C. Wu, A. Bertrand, E. Graham, J. Schoonbaert, S. Giannoukos, U. Baltensperger, A. S. H. Prevot, I. Riipinen, I. El Haddad and C. Mohr, Particle-phase processing of α-pinene NO_3 secondary organic aerosol in the dark, *Atmos. Chem. Phys.*, 2022, **22**, 13167–13182.

34 D. Grosjean, E. Grosjean, J. H. Seinfeld and T. Novakov, Atmospheric oxidation of terpenes: gas phase products and aerosol formation, *Abstr. Pap. Am. Chem. Soc.*, 1994, **207**, 159.

35 J. Hammes, A. Lutz, T. Mentel, C. Faxon and M. Hallquist, Carboxylic acids from limonene oxidation by ozone and hydroxyl radicals: insights into mechanisms derived using a FIGAERO-CIMS, *Atmos. Chem. Phys.*, 2019, **19**, 13037–13052.

36 V. Pospisilova, D. M. Bell, H. Lamkaddam, A. Bertrand, L. Wang, D. Bhattu, X. Zhou, J. Dommen, A. S. H. Prevot, U. Baltensperger, I. El Haddad and J. G. Slowik, Photodegradation of alpha-Pinene Secondary Organic Aerosol Dominated by Moderately Oxidized Molecules, *Environ. Sci. Technol.*, 2021, **55**, 6936–6943.

37 C. Rösch, D. K. Wissenbach, U. Franck, M. Wendisch and U. Schlink, Degradation of indoor limonene by outdoor ozone: a cascade of secondary organic aerosols, *Environ. Pollut.*, 2017, **226**, 463–472.

38 K. Loven, C. Isaxon, A. Wierzbicka and A. Gudmundsson, Characterization of airborne particles from cleaning sprays and their corresponding respiratory deposition fractions, *J. Occup. Environ. Hyg.*, 2019, **16**, 656–667.

39 A. Manoukian, E. Quivet, B. Temime-Roussel, M. Nicolas, F. Maupetit and H. Wortham, Emission characteristics of air pollutants from incense and candle burning in indoor atmospheres, *Environ. Sci. Pollut. Res.*, 2013, **20**, 4659–4670.

40 L. Morawska, G. A. Ayoko, G. N. Bae, G. Buonanno, C. Y. H. Chao, S. Clifford, S. C. Fu, O. Hänninen, C. He, C. Isaxon, M. Mazaheri, T. Salthammer, M. S. Waring and A. Wierzbicka, Airborne particles in indoor environment of homes, schools, offices and aged care facilities: the main routes of exposure, *Environ. Int.*, 2017, **108**, 75–83.

41 L. Morawska, A. Afshari, G. N. Bae, G. Buonanno, C. Y. Chao, O. Hanninen, W. Hofmann, C. Isaxon, E. R. Jayaratne, P. Pasanen, T. Salthammer, M. Waring and A. Wierzbicka, Indoor aerosols: from personal exposure to risk assessment, *Indoor Air*, 2013, **23**, 462–487.

42 P. Wolkoff, Indoor air chemistry: terpene reaction products and airway effects, *Int. J. Hyg. Environ. Health*, 2020, **225**, 113439.

43 T. Rönkkö, H. Kuuluvainen, P. Karjalainen, J. Keskinen, R. Hillamo, J. V. Niemi, L. Pirjola, H. J. Timonen, S. Saarikoski, E. Saukko, A. Järvinen, H. Silvennoinen, A. Rostedt, M. Olin, J. Yli-Ojanperä, P. Nousiainene, A. Kousa and M. Dal Maso, Traffic is a major source of atmospheric nanocluster aerosol, *Proc. Natl. Acad. Sci. U.S.A.*, 2017, **114**, 7549–7554.

44 H. F. Hubbard, B. K. Coleman, G. Sarwar and R. L. Corsi, Effects of an ozone-generating air purifier on indoor secondary particles in three residential dwellings, *Indoor Air*, 2005, **15**, 432–444.

45 E. Gomez Alvarez, D. Amedro, C. Afif, S. Gligorovski, C. Schoemaecker, C. Fittschen, J. F. Doussin and H. Wortham, Unexpectedly high indoor hydroxyl radical concentrations associated with nitrous acid, *Proc. Natl. Acad. Sci. U.S.A.*, 2013, **110**, 13294–13299.

46 A. Gandolfo, V. Gligorovski, V. Bartolomei, S. Tlili, E. Gómez Alvarez, H. Wortham, J. Kleffmann and S. Gligorovski, Spectrally resolved actinic flux and photolysis frequencies of key species within an indoor environment, *Building and Environment*, 2016, **109**, 50–57.

47 H. Deng, X. Xu, K. Wang, J. Xu, G. Loisel, Y. Wang, H. Pang, P. Li, Z. Mai, S. Yan, X. Li and S. Gligorovski, The Effect of Human Occupancy on Indoor Air Quality through Real-

Time Measurements of Key Pollutants, *Environ. Sci. Technol.*, 2022, **56**, 15377–15388.

48 F. D. Lopez-Hilfiker, V. Pospisilova, W. Huang, M. Kalberer, C. Mohr, G. Stefenelli, J. A. Thornton, U. Baltensperger, A. S. H. Prevot and J. G. Slowik, An extractive electrospray ionization time-of-flight mass spectrometer (EESI-TOF) for online measurement of atmospheric aerosol particles, *Atmos. Meas. Tech.*, 2019, **12**, 4867–4886.

49 W. Wang, Y. H. Zhang, B. Jiang, Y. Y. Chen, Y. Y. Song, Y. T. Tang, C. Dong and Z. W. Cai, Molecular characterization of organic aerosols in Taiyuan, China: Seasonal variation and source identification, *Sci. Total Environ.*, 2021, **800**, 149419.

50 I. Kourtchev, R. H. M. Godoi, S. Connors, J. G. Levine, A. T. Archibald, A. F. L. Godoi, S. L. Paralovo, C. G. G. Barbosa, R. A. F. Souza, A. O. Manzi, R. Seco, S. Sjostedt, J.-H. Park, A. Guenther, S. Kim, J. Smith, S. T. Martin and M. Kalberer, Molecular composition of organic aerosols in central Amazonia: an ultra-high-resolution mass spectrometry study, *Atmos. Chem. Phys.*, 2016, **16**, 11899–11913.

51 P. Tu, W. A. t. Hall and M. V. Johnston, Characterization of Highly Oxidized Molecules in Fresh and Aged Biogenic Secondary Organic Aerosol, *Anal. Chem.*, 2016, **88**, 4495–4501.

52 L. R. Mazzoleni, P. Saranjampour, M. M. Dalbec, V. Samburova, A. G. Hallar, B. Zielinska, D. H. Lowenthal and S. Kohl, Identification of water-soluble organic carbon in non-urban aerosols using ultrahigh-resolution FT-ICR mass spectrometry: organic anions, *Environ. Chem.*, 2012, **9**, 285–297.

53 I. Kourtchev, S. J. Fuller, C. Giorio, R. M. Healy, E. Wilson, I. O'Connor, J. C. Wenger, M. McLeod, J. Aalto, T. M. Ruuskanen, W. Maenhaut, R. Jones, D. S. Venables, J. R. Sodeau, M. Kulmala and M. Kalberer, Molecular composition of biogenic secondary organic aerosols using ultrahigh-resolution mass spectrometry: comparing laboratory and field studies, *Atmos. Chem. Phys.*, 2014, **14**, 2155–2167.

54 X. Xu, H. W. Pang, C. Liu, K. Y. Wang, G. Loisel, L. Li, S. Gligorovski and X. Li, Real-time measurements of product compounds formed through the reaction of ozone with breath exhaled VOCs, *Environ. Sci.: Processes Impacts*, 2022, **24**, 2237–2248.

55 T. Berndt, S. Richters, T. Jokinen, N. Hyttinen, T. Kurtén, R. V. Otkjær, H. G. Kjaergaard, F. Stratmann, H. Herrmann, M. Sipilä, M. Kulmala and M. Ehn, Hydroxyl radical-induced formation of highly oxidized organic compounds, *Nat. Commun.*, 2016, **7**, 13677.

56 M. Ehn, J. A. Thornton, E. Kleist, M. Sipilä, H. Junninen, I. Pullinen, M. Springer, F. Rubach, R. Tillmann, B. Lee, F. Lopez-Hilfiker, S. Andres, I. H. Acir, M. Rissanen, T. Jokinen, S. Schobesberger, J. Kangasluoma, J. Kontkanen, T. Nieminen, T. Kurtén, L. B. Nielsen, S. Jorgensen, H. G. Kjaergaard, M. Canagaratna, M. Dal Maso, T. Berndt, T. Petäjä, A. Wahner, V. M. Kerminen, M. Kulmala, D. R. Worsnop, J. Wildt and T. F. Mentel, A large source of low-volatility secondary organic aerosol, *Nature*, 2014, **506**, 476.

57 D. Pagonis, L. B. Algrim, D. J. Price, D. A. Day, A. V. Handschy, H. Stark, S. L. Miller, J. A. de Gouw, J. L. Jimenez and P. J. Ziemann, Autoxidation of Limonene Emitted in a University Art Museum, *Atmos. Meas. Tech.*, 2019, **6**, 520–524.

58 U. Molteni, M. Simon, M. Heinritzi, C. R. Hoyle, A.-K. Bernhammer, F. Bianchi, M. Breitenlechner, S. Brilke, A. Dias, J. Duplissy, C. Frege, H. Gordon, C. Heyn, T. Jokinen, A. Kürten, K. Lehtipalo, V. Makhmutov, T. Petäjä, S. M. Pieber, A. P. Praplan, S. Schobesberger, G. Steiner, Y. Stozhkov, A. Tomé, J. Tröstl, A. C. Wagner, R. Wagner, C. Williamson, C. Yan, U. Baltensperger, J. Curtius, N. M. Donahue, A. Hansel, J. Kirkby, M. Kulmala, D. R. Worsnop and J. Dommen, Formation of Highly Oxygenated Organic Molecules from α-Pinene Ozonolysis: Chemical Characteristics, Mechanism, and Kinetic Model Development, *ACS Earth Space Chem.*, 2019, **3**, 873–883.

59 K. Pytel, R. Marcinkowska, M. L. Rutkowska and B. Zabiegala, Recent advances on SOA formation in indoor air, fate and strategies for SOA characterization in indoor air-A review, *Sci. Total Environ.*, 2022, **843**, 156948.

60 F. Bianchi, T. Kurtén, M. Riva, C. Mohr, M. P. Rissanen, P. Roldin, T. Berndt, J. D. Crounse, P. O. Wennberg, T. F. Mentel, J. Wildt, H. Junninen, T. Jokinen, M. Kulmala, D. R. Worsnop, J. A. Thornton, N. Donahue, H. G. Kjaergaard and M. Ehn, Highly Oxygenated Organic Molecules (HOM) from Gas-Phase Autoxidation Involving Peroxy Radicals: A Key Contributor to Atmospheric Aerosol, *Chem. Rev.*, 2019, **119**, 3472–3509.

61 R. Teraoka, M. Otsuka and Y. Matsuda, Chemical-Stability Of Ethyl Icosapentate Against Autoxidation. 2. Effect Of Photoirradiation On Oxidation-Kinetics, *Pharm. Res.*, 1994, **11**, 1077–1081.

62 M. S. H. Salem, C. Dubois, Y. Takamura, A. Kitajima, T. Kawai, S. Takizawa and M. Kirihara, Light-induced autoxidation of aldehydes to peracids and carboxylic acids, *Green Chem.*, 2024, **26**, 375–383.

63 K. E. Fygle and T. B. Melo, Optical absorption studies of the kinetics of UV- and self-initiated autoxidation of linoleate micelles, *Chem. Phys. Lipids*, 1996, **79**, 39–46.

64 M. J. Pavan, H. Fridman, G. Segalovich, A. I. Shames, N. G. Lemcoff and T. Mokari, Photoxidation of Benzyl Alcohol with Heterogeneous Photocatalysts in the UV Range: The Complex Interplay with the Autoxidative Reaction, *ChemCatChem*, 2018, **10**, 2541–2545.

65 J. He, H. Zhang, W. X. Wang, Y. X. Ma, M. Yang, Y. W. He, Z. Liu, K. Yu and J. Jiang, Probing autoxidation of oleic acid at air–water interface: a neglected and significant pathway for secondary organic aerosols formation, *Environ. Res.*, 2022, **212**, 113232.

66 E. Viinanen and A. Hopia, Reversed-Phase High-Performance Liquid-Chromatographic Analysis Of Triacylglycerol Autoxidation Products With Ultraviolet And

Evaporative Light-Scattering Detectors, *J. Am. Oil Chem. Soc.*, 1994, **71**, 537–539.

67 R. K. Pathak, K. Salo, E. U. Emanuelsson, C. L. Cai, A. Lutz, Å. Hallquist and M. Hallquist, Influence of Ozone and Radical Chemistry on Limonene Organic Aerosol Production and Thermal Characteristics, *Environ. Sci. Technol.*, 2012, **46**, 11660–11669.

68 N. Carslaw, A mechanistic study of limonene oxidation products and pathways following cleaning activities, *Atmos. Environ.*, 2013, **80**, 507–513.

69 A. Tekle-Röttering, S. Lim, E. Reisz, H. V. Lutze, M. S. Abdighahroudi, S. Willach, W. Schmidt, P. R. Tentscher, D. Rentsch, C. S. McArdell, T. C. Schmidt and U. von Gunten, Reactions of pyrrole, imidazole, and pyrazole with ozone: kinetics and mechanisms, *Environ. Sci.: Water Res. Technol.*, 2020, **6**, 976–992.

70 W. Yiqun, H. Deng, L. Pan, J. Xu, G. Loisel, H. Pang, X. Xu, X. Li and S. Gligorovski, Interfacial Ozone Oxidation Chemistry at a Riverine Surface Microlayer as a Source of Nitrogen Organic Compounds, *Atmos. Meas. Tech.*, 2022, **9**, 493–500.

71 Y. Q. Wang, H. F. Deng, P. Li, J. L. Xu, B. Jiang, H. W. Pang and S. Gligorovski, Molecular Characterization of the Product Compounds Formed Upon Heterogeneous Chemistry of Ozone With Riverine Surface Microlayer, *J. Geophys. Res.: Atmos.*, 2022, **127**, e2022JD037182.

72 J. D. Surratt, Y. Gómez-González, A. W. H. Chan, R. Vermeylen, M. Shahgholi, T. E. Kleindienst, E. O. Edney, J. H. Offenberg, M. Lewandowski, M. Jaoui, W. Maenhaut, M. Claeys, R. C. Flagan and J. H. Seinfeld, Organosulfate Formation in Biogenic Secondary Organic Aerosol, *J. Phys. Chem. A*, 2008, **112**, 8345–8378.

73 Y. Wan, X. Huang, B. Jiang, B. Kuang, M. Lin, D. Xia, Y. Liao, J. Chen, J. Z. Yu and H. Yu, Probing key organic substances driving new particle growth initiated by iodine nucleation in coastal atmosphere, *Atmos. Chem. Phys.*, 2020, **20**, 9821–9835.

74 D. M. Cai, X. K. Wang, C. George, T. T. Cheng, H. Herrmann, X. Li and J. M. Chen, Formation of Secondary Nitroaromatic Compounds in Polluted Urban Environments, *J. Geophys. Res.: Atmos.*, 2022, **127**, e2021JD036167.

75 S. Kim, R. W. Kramer and P. G. Hatcher, Graphical Method for Analysis of Ultrahigh-Resolution Broadband Mass Spectra of Natural Organic Matter, the Van Krevelen Diagram, *Anal. Chem.*, 2003, **75**, 5336–5344.

76 K. J. Nihill, M. M. Coggon, C. Y. Lim, A. R. Koss, B. Yuan, J. E. Krechmer, K. Sekimoto, J. L. Jimenez, J. de Gouw, C. D. Cappa, C. L. Heald, C. Warneke and J. H. Kroll, Evolution of organic carbon in the laboratory oxidation of biomass-burning emissions, *Atmos. Chem. Phys.*, 2023, **23**, 7887–7899.

77 Y. Wang, M. Hu, P. Lin, T. Tan, M. Li, N. Xu, J. Zheng, Z. Du, Y. Qin, Y. Wu, S. Lu, Y. Song, Z. Wu, S. Guo, L. Zeng, X. Huang and L. He, Enhancement in Particulate Organic Nitrogen and Light Absorption of Humic-Like Substances over Tibetan Plateau Due to Long-Range Transported Biomass Burning Emissions, *Environ. Sci. Technol.*, 2019, **53**, 14222–14232.

78 P. Lin, A. G. Rincon, M. Kalberer and J. Z. Yu, Elemental composition of HULIS in the Pearl River Delta Region, China: results inferred from positive and negative electrospray high resolution mass spectrometric data, *Environ. Sci. Technol.*, 2012, **46**, 7454–7462.

79 J. C. Ditto, J. Machesky and D. R. Gentner, Analysis of reduced and oxidized nitrogen-containing organic compounds at a coastal site in summer and winter, *Atmos. Chem. Phys.*, 2022, **22**, 3045–3065.

80 E. J. Palen, D. T. Allen, S. N. Pandis, S. E. Paulson, J. H. Seinfeld and R. C. Flagan, Fourier-Transform Infrared-Analysis Of Aerosol Formed In The Photooxidation Of Isoprene And Beta-Pinene, *Atmos. Environ., Part A*, 1992, **26**, 1239–1251.

81 Y. Wang, M. Mekic, P. Li, H. Deng, S. Liu, B. Jiang, B. Jin, D. Vione and S. Gligorovski, Ionic Strength Effect Triggers Brown Carbon Formation through Heterogeneous Ozone Processing of *Ortho*-Vanillin, *Environ. Sci. Technol.*, 2021, **55**, 4553–4564.

82 X. Tang, P. K. Misztal, W. W. Nazaroff and A. H. Goldstein, Volatile Organic Compound Emissions from Humans Indoors, *Environ. Sci. Technol.*, 2016, **50**, 12686–12694.

83 X. Wang, N. Hayeck, M. Brüggemann, L. Yao, H. Chen, C. Zhang, C. Emmelin, J. Chen, C. George and L. Wang, Chemical Characteristics of Organic Aerosols in Shanghai: A Study by Ultrahigh-Performance Liquid Chromatography Coupled With Orbitrap Mass Spectrometry, *J. Geophys. Res.: Atmos.*, 2017, **122**, 11703–11722.

84 S. S. Yu, L. Jia, Y. F. Xu and Y. P. Pan, Molecular composition of secondary organic aerosol from styrene under different NOx and humidity conditions, *Atmos. Res.*, 2022, **266**, 105950.

85 X. Lu, M. Qin, P. H. Xie, J. Duan, W. Fang and W. Q. Liu, Observation of ambient NO3 radicals by LP-DOAS at a rural site in North China Plain, *Sci. Total Environ.*, 2022, **804**, 149680.

86 E. Aruffo, J. F. Wang, J. H. Ye, P. Ohno, Y. M. Qin, M. Stewart, K. McKinney, P. Di Carlo and S. T. Martin, Partitioning of Organonitrates in the Production of Secondary Organic Aerosols from α-Pinene Photo-Oxidation, *Environ. Sci. Technol.*, 2022, **56**, 5421–5429.

87 L. D. Yee, G. Isaacman-VanWertz, R. A. Wernis, N. M. Kreisberg, M. Glasius, M. Riva, J. D. Surratt, S. S. de Sá, S. T. Martin, M. L. Alexander, B. B. Palm, W. W. Hu, P. Campuzano-Jost, D. A. Day, J. L. Jimenez, Y. J. Liu, P. K. Misztal, P. Artaxo, J. Viegas, A. Manzi, R. A. F. de Souza, E. S. Edgerton, K. Baumann and A. H. Goldstein, Natural and Anthropogenically Influenced Isoprene Oxidation in Southeastern United States and Central Amazon, *Environ. Sci. Technol.*, 2020, **54**, 5980–5991.

88 H. Greim, D. Bury, H. J. Klimisch, M. Oeben-Negele and K. Ziegler-Skylakakis, Toxicity of aliphatic amines: Structure–activity relationship, *Chemosphere*, 1998, **36**, 271–295.